

Evidence of Ferromagnetic Short-Range Correlations in Sol-gel Synthesized $\text{La}_{1.88}\text{Sr}_{0.12}\text{CoMnO}_6$ Nanoparticles



Swati Jharwal and Arvind Kumar

1 Introduction

Oxide-based double perovskite compounds with crystal formula, $\text{A}_2\text{BB}'\text{O}_6$ have attracted the attention of researchers in the last two decades due to multifunctional properties exhibited by these compounds [1]. Double perovskite compounds were found to display interesting magnetic properties such as near room temperature ferromagnetism, colossal magneto-resistance, magneto-dielectric, etc., which have potential applications for the spintronic devices [2]. In comparison to oxide-based single perovskites of ABO_3 type, the double perovskites have another element at B-site (B') [3]. This structural modification, i.e., different orders of ions at B-site produce multiple exchange interactions resulting from different oxidation states of B-site ions exhibited in different crystal symmetry and lattice distortions give rise to many of the functional properties for the compound [4, 5]. In the recent past lead-free inorganic perovskite structures are widely studied due to the need of clean and green technological advancements [3–9].

Among the various studied double perovskite materials, La-based double perovskites $\text{La}_2\text{CoMnO}_6$ (LCMO) and $\text{La}_2\text{NiMnO}_6$ (LNMO) are widely studied by researchers due to the magnetodielectric, magnetoresistance, and magnetocapacitance properties for possible application in spintronic devices [6]. They exhibit interesting magnetic properties owing to their multiple oxidation state in B/Mn ordering [7]. LNMO is a ferromagnetic semiconductor with paramagnetic to ferromagnetic transition near room temperature ~ 275 K [8]. $\text{La}_2\text{CoMnO}_6$ (LCMO) is known to be a ferromagnetic insulator which in its ordered state shows a ferromagnetic transition

S. Jharwal · A. Kumar (✉)

Materials Science Research Lab (Theory and Experimental, Department of Physics, ARSD College, University of Delhi, New Delhi 110021, India

e-mail: bhuarvind2512@gmail.com; arvindkumar@arsd.du.ac.in; arvind@jnu.ac.in

A. Kumar

School of Physical Sciences, Jawaharlal Nehru University, New Delhi 110067, India

about 240 K due to the super-exchange interaction of $\text{Co}^{2+}-\text{O}^{2-}-\text{Mn}^{4+}$ ions where Mn appears in its high spin state [9]. In its disordered state Co and Mn also appear in +3 charge state due to which the ferromagnetic transition is around 150 K [9]. When the A site of the compound $\text{A}_2\text{BB}'\text{O}_6$ is doped with holes, i.e., when Sr^{2+} replaces La^{3+} in LCMO, it is interesting to study the effect of anti-site disorder created in an otherwise ordered perovskite on the magnetic properties of the system [10]. In addition to the chemical disorder created by the doping, the manganite's structural disorder is also there because of Jahn Teller distortions and octahedral tilt [11]. Due to structural distortion, the interaction among the magnetic ions (B-Site ion) at the centre of the octahedra is also affected because the distortion of the structure leads to a change in the degree of overlap of the t_{2g} and e_g orbitals of the transition metal ion. As a result of which the occupying electrons take the type of magnetic configuration which saves maximum energy [12]. The exhibited magnetic properties as a result of interplay of structural and chemical disorder are worth studying. Aga Shahee et al has reported the existence of ferromagnetic correlations above the anti-ferromagnetic ordering temperatures at ~ 368 K for cubic perovskite manganite's [11]. Such ferromagnetic correlations are important from the point of view of application in the field of spintronics.

In this paper we have studied the magnetic interactions in LCMO and Sr doped LCMO nanoparticles synthesized by sol-gel method through temperature-dependent magnetization study and have observed the ferromagnetic short-range correlations in LSCMO nanoparticles formed in rhombohedral phase.

2 Experimental Details

2.1 Synthesis Details

Pure, $\text{La}_2\text{CoMnO}_6$ (LCMO) and Sr doped $\text{La}_{2-x}\text{Sr}_x\text{CoMnO}_6$ (LSCMO: $x = 0.12$) nanoparticles were synthesized by the sol-gel method. In the preparation of nanoparticles, nitrate precursors $\text{La}(\text{NO}_3)_3 \cdot \text{Co}(\text{NO}_3)_2 \cdot 6\text{H}_2\text{O}$, $\text{Sr}(\text{NO}_3)_2$ and $\text{Mn}(\text{NO}_3)_2$ were taken in stoichiometric ratio and dissolved in 100 ml of deionized water. Citric acid was added in the solution as the capping agent. The solution was further stirred continuously on a magnetic stirrer by maintaining a constant temperature of 70°C till a viscous gel is obtained. The obtained gel was dried in a hot air oven at 150°C for about 6 h to obtain a dry fluffy powder. The powder was ground in an agate mortar to obtain a very fine powder. This powder was kept for calcination in a muffle furnace at 600°C for 4 h. The obtained black powder was ground and collected for further investigation of the physical properties via different experimental techniques. Figure 1 shows schematically the different steps in the synthesis of Sr doped LCMO nanoparticles by sol-gel method. The corresponding chemical reaction is as follows;



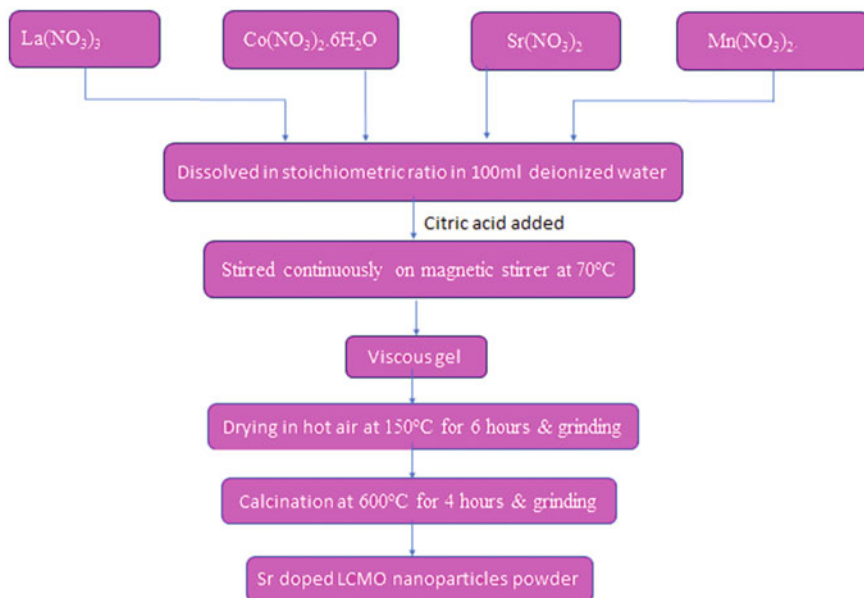
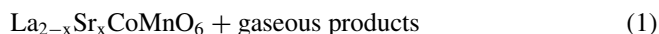


Fig. 1 Schematic representation of steps of synthesis by sol-gel method to prepare LCMO and LSCMO nanoparticles



2.2 Characterization Techniques

X-ray diffraction spectra was recorded from Bruker D8 X-ray diffractometer using Cu-K α source ($\lambda = 1.54060 \text{ \AA}$) to analyze the structural properties of the prepared nanoparticles of LCMO and LSCMO. To study the structural phase formation and bonding nature, Fourier transform infrared (FTIR) with attenuated total reflectance (ATR-FTIR, Bruker Tech.) and Raman spectroscopy were used. Raman Spectra was recorded with an excitation source of wavelength 514 nm of air-cooled Argon ion laser. Laser power at the sample was $\sim 4 \text{ mW}$ and typical spectral acquisition time was $\sim 50 \text{ s}$ with the spectral resolution of 1 cm^{-1} . To investigate the detailed magnetic properties, M-H curve at different temperature was recorded using the Quantum Design SQUID-VSM (VSM, Versa Lab) from 60 to 300 K.

3 Results and Discussion

3.1 Structural Study and Strain Calculation

Figure 2 shows the XRD pattern of LCMO and LSCMO nanoparticles. The peaks of XRD are indexed (JCPDS file no #53–1211) with proper (hkl) planes and confirm the formation of the desired nanoparticles. The peak positions in XRD pattern of LSCMO nanoparticles are slightly shifted toward the higher angle side compared to peak positions of LCMO nanoparticles. From Table 1 we can observe widening and shifting of the diffraction peaks with Sr doping indicating the replacement of the La ions with Sr ions in the LCMO host lattice. The crystallite size has also been estimated from Scherrer formula [13] and found to be in the range of 6–18 nm as tabulated in Table 1. It has also been observed that along with the widening and shifting of the diffraction peaks the synthesized materials are within the nanometer range. XRD pattern of the LSCMO shows that the full width at half-maximum (FWHM) of most of the peaks increases with a doping percentage of Sr which can be attributed to a decrease in crystallite size (Table 3).

To collect more information regarding the structural phase formed and other lattice parameters, the Rietveld refinement of X-ray diffraction pattern using FullProf software was carried out. Figure 3 shows the Rietveld refinement plots of LCMO and LSCMO nanoparticles. For the refinement procedure, initial input parameters (such as unit cell lattice parameters, space group and atom coordinates) are taken from matching reference patterns [14]. The pseudo-voigt function has been chosen in the present study for peak shapes in the refinement purpose. It has been found from Fig. 3 that observed and calculated patterns are in good agreement to each other. The X-ray diffraction pattern after refinement corresponds to rhombohedral structure (space group $R3c$ (161)). Table 2 lists the Wyckoff positions, lattice parameters and bond distances obtained from refinement. The value of parameters for LSCMO

Fig. 2 X-ray diffraction pattern of the synthesized LCMO and LSCMO for nanoparticles

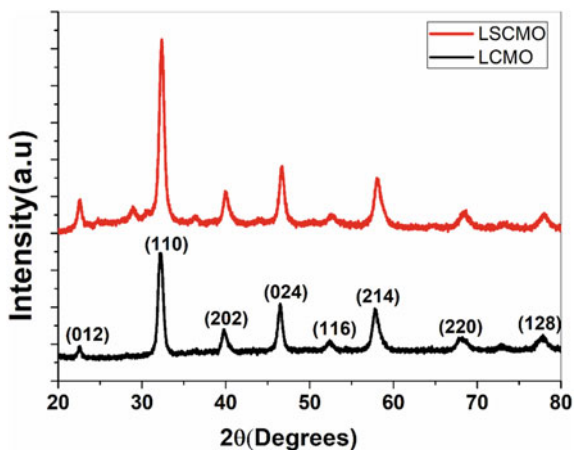
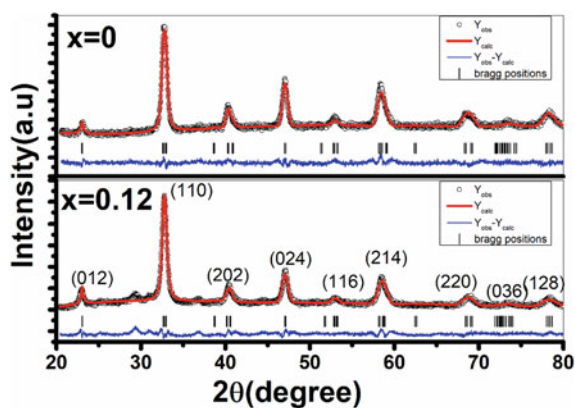


Table 1 Comparison of 2θ position and FWHM values of XRD peaks of XRD of LCMO and LSCMO nanoparticles

2θ positions of XRD peaks		FWHM (degrees)		Crystallite size (Scherrer formula)	
LCMO	LSCMO	LCMO	LSCMO	LCMO	LSCMO
22.54	22.57	0.46	0.50	17.66	16.13
32.23	32.36	0.73	0.76	11.30	10.89
39.84	40.04	0.75	0.79	11.18	10.73
46.49	46.68	0.71	0.73	12.08	11.81
57.90	58.15	1.07	1.10	8.51	8.24
68.18	68.42	1.50	1.24	6.39	7.73
77.77	77.93	1.26	1.06	8.09	9.67

Fig. 3 Rietveld refinement of X-ray diffraction pattern of pure and Sr doped $\text{La}_2\text{CoMnO}_6$ nanoparticles. Observed (black dots), calculated (red solid line), and difference (blue line at the bottom) profiles. The black tick marks indicate the positions of the allowed Bragg reflections



varies slightly from LCMO which could be attributed to different ionic radii of Sr (1.13 \AA) and La (1.06 \AA) [14].

Induced strain (ϵ) in the prepared LCMO and LSCMO nanoparticles due to some distortions is estimated by plotting Williamson–Hall (W–H) plots as shown in Fig. 4a, b. The values of estimated crystallite size and strain are tabulated in Table 3. The crystallite size obtained from W–H plots is larger compared to values obtained by Debye Scherrer formula as the effect of broadening of peaks due to strain is not considered in it. It has been observed that the value of estimated strain in LSCMO sample is less as compared to the pure LCMO sample and the difference in the crystallite size measurement from Debye Scherrer formula and W–H plots is smaller in this case.

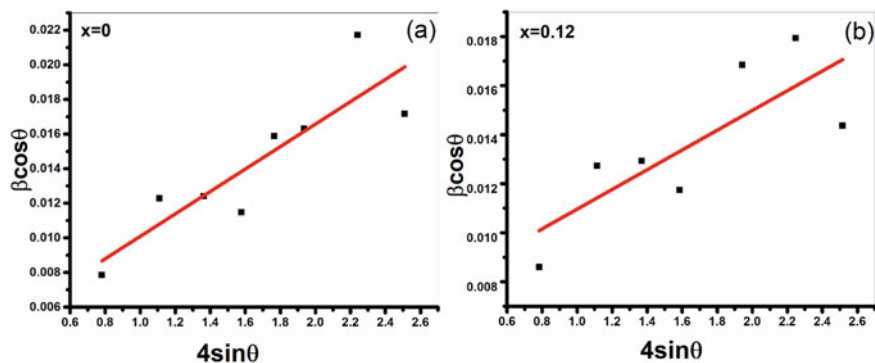


Fig. 4 a, b Williamson Hall (W-H) plots for the pure and Sr doped LCMO nanoparticles

Table 2 Structural parameters obtained from Rietveld analysis of LCMO and LSCMO nanoparticles

Parameters	x = 0	x = 0.12
Atomic positions	La:6a(0,0,0.250)	La:6a(0,0, 0.24961)
	Co/Mn:6a(0,0,0)	Co/Mn:6a(0,0, 0.0147)
	O:18b(0.457,0,0.252)	O:18b(0.5405,0,0.741)
Lattice parameters		
a	5.48 Å	5.44
b	5.48 Å	5.44
c	13.25 Å	13.47
d ₁₁₀	2.74 Å	2.72
La/Sr-O(Å)	2.73	2.73
Co/Mn-O(Å)	1.94	1.96
χ ²	1.7	3.12

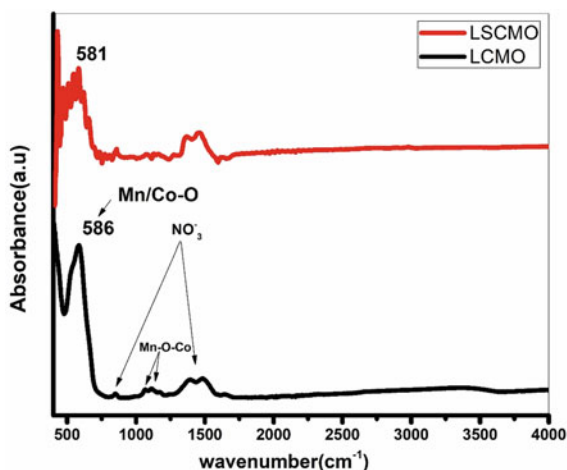
Table 3 Crystallite size and strain obtained from W-H plots for LCMO and Sr doped LCMO compound

Doping concentration (x)	Crystallite size (nm) (By Scherrer formula)	Crystallite size(nm) (W-H Plots)	Strain (calculated from W-H plots)
0	11.30	38.4	6.48×10^{-3}
0.12	10.89	19.97	4.02×10^{-3}

3.2 FTIR Spectroscopy Analysis

FTIR spectra of the material give insights about the attached functional groups and impurities present [15]. Figure 5 shows the absorbance spectra obtained for LCMO

Fig. 5 FTIR spectra of LCMO and LSCMO nanoparticles in absorbance mode

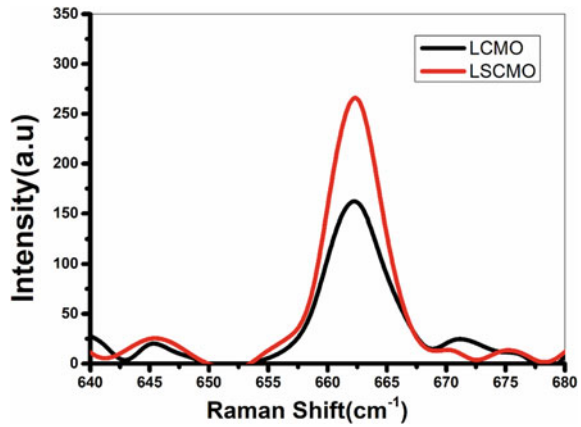


and LSCMO nanoparticles in the wavenumber range of 400–4000 cm^{-1} recorded at room temperature (RT) [16]. A strong band at 586 cm^{-1} for the LCMO nanoparticles is obtained which is due to Co–O/Mn–O vibrations in LCMO nanoparticles. Some weak bands are also obtained around 1073 cm^{-1} and 1145 cm^{-1} which could be due to Mn–O–Co vibration in MnO_6 octahedra. Weak bands are also obtained at 1393 cm^{-1} and about 855 cm^{-1} which corresponds to vibration of nitrate ions [17]. The bands obtained at 1483 cm^{-1} could be due to vibration of N–O from the nitrate precursors taken [18]. In the LSCMO nanoparticles a strong band is observed at 581 cm^{-1} , i.e., the bands are shifted to lower wave number side with the doping of Sr in the LCMO lattice.

3.3 Raman Spectroscopy Study

Raman spectra of the material is an efficient way of detecting the phases present. The peaks in the spectrum at different wavelengths are corresponding to specific vibration of molecular bonds and lattices [15]. In double perovskite compounds ($\text{A}_2\text{BB}'\text{O}_6$) structure, the vibrational modes are due to BO_6 and $\text{B}'\text{O}_6$ octahedra and A–O bonds [19]. Figure 6 shows the Raman spectra of LCMO and LSCMO nanoparticles recorded at RT at an excitation wavelength of 514 nm. The spectra show a peak at $\sim 662 \text{ cm}^{-1}$ for LCMO and with a slight shifting in case of LSCMO which is due to the incorporation of Sr^{+2} ions in host LCMO. The observed peak in the spectra is due to A_{1g} symmetric stretching vibration mode of oxygen octahedra around cations [20, 21].

Fig. 6 Raman spectra of LCMO and LSCMO nanoparticles



3.4 Magnetic Measurements

Figure 7 plots magnetization as a function of magnetic field for LCMO and LSCMO nanoparticles at RT by varying magnetic field from $-30,000$ Oe to $+30,000$ Oe. The inset of Fig. 7 shows the M-H curve in low magnetic field region from -2700 Oe to $+2700$ Oe. The nature of M-H curves of LCMO and LSCMO nanoparticles indicate dominant paramagnetic nature of the double perovskites at room temperature. The magnetic parameters: maximum magnetization (M_s), coercivity (H_c) and retentivity (M_r) obtained from M-H data (Fig. 7) are tabulated in Table 4. The value of M_s and M_r for LSCMO was found to be increased whereas the value of H_c decreased for the LSCMO nanoparticles as compared to LCMO nanoparticles.

Figure 8a shows M-H curves recorded at various temperatures for LCMO and LSCMO nanoparticles. This also indicates an increase in maximum magnetization and coercivity at low temperature with Sr doping in LCMO host lattice. From Fig. 8a we can see that the LCMO and LSCMO nanoparticles undergo a transition to ferromagnetic behavior below room temperature from paramagnetic behavior shown at room temperature. Figure 8b represents the Zero field cooled (ZFC: black color) and field cooled (FC: red color) magnetization curve of LCMO and LSCMO nanoparticles in the temperature range 60–400 K. To know exactly the transition temperature, the first derivative of the ZFC magnetization as a function of temperature (inset of Fig. 8b), i.e., dM/dT Vs T graph for LCMO nanoparticles was plotted which indicates two transition temperatures at ~ 220 and ~ 175 K. Anomaly was observed at further lower temperatures around 100–115 K, which could be attributed to the glassy behavior indicated as T_{fg} [24]. The observed transition at ~ 220 K and at ~ 175 K could be due to $\text{Co}^{2+}-\text{O}^{2-}-\text{Mn}^{4+}$ ferromagnetic super exchange interactions and $\text{Co}^{3+}-\text{O}^{2-}-\text{Mn}^{4+}$ ferromagnetic super exchange interactions, respectively [22, 23]. The ZFC-FC and dM/dT versus T graph (inset of Fig. 8b) plots for LSCMO ($x = 0.12$) nanoparticles indicate one prominent transition temperature at 175 K and a small minimum is obtained around ~ 360 K. This implies that with the doping of Sr

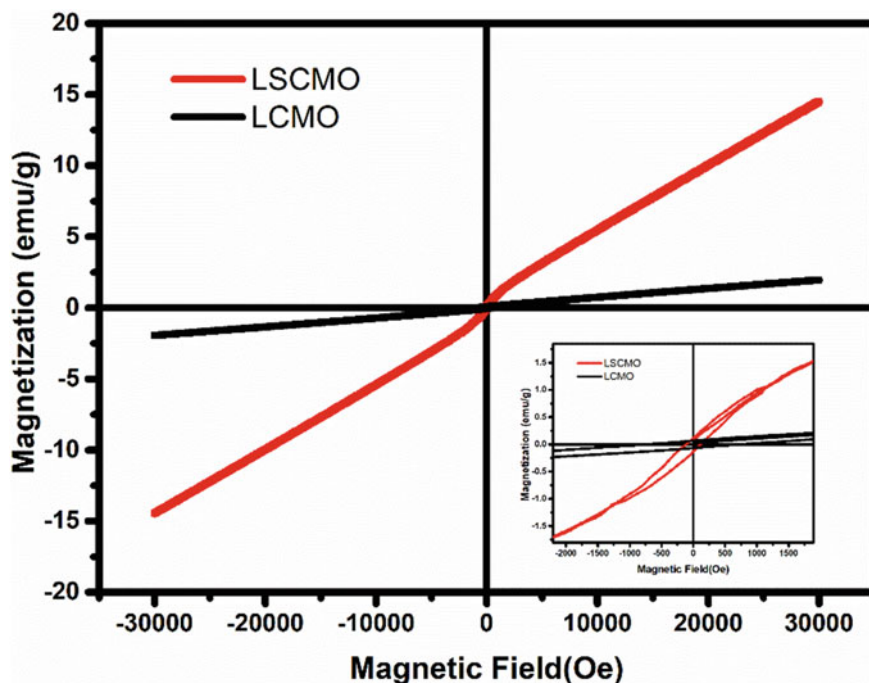


Fig. 7 Room temperature magnetization (M–H) curve of LCMO and LSCMO nanoparticles

Table 4 Magnetic parameters obtained from the M–H experimental curve

Composition	Remnant magnetization (M_r) (emu/g)	Maximum magnetization (M_s) (emu/g)	Coercivity values (H_c) (Oe)
$\text{La}_2\text{CoMnO}_6$	0.07	1.96	737.94
$\text{La}_{1.88}\text{Sr}_{0.12}\text{CoMnO}_6$	0.12	14.50	112.58

in LCMO nanoparticles the effect of ferromagnetic ordering due to $\text{Co}^{2+}\text{--O}^{2-}\text{--Mn}^{4+}$ super exchange interaction is reduced and due to $\text{Co}^{3+}\text{--O}^{2-}\text{--Mn}^{4+}$ ferromagnetic super exchange interactions are enhanced [10]. The existence of lower transition temperature in case of LSCMO indicates that Co^{3+} and Mn^{3+} exist whereas ideally only Co^{2+} and Mn^{4+} ions are expected in LCMO system [9].

In order to get more insight about the magnetic transition temperature of the compounds inverse of susceptibility was plotted as a function of temperature (Fig. 9). On extrapolating the linear portion of the inverse susceptibility for LCMO nanoparticles it intersects x-axis at about ~ 220 K. The linear portion of the graph beyond this temperature indicates paramagnetic nature in accordance with Curie–Weiss law [12]. For LSCMO ($x = 0.12$) nanoparticles the inverse susceptibility graph has two linear regions which on extrapolating intersect the x-axis at 350 K and ~ 175 K.

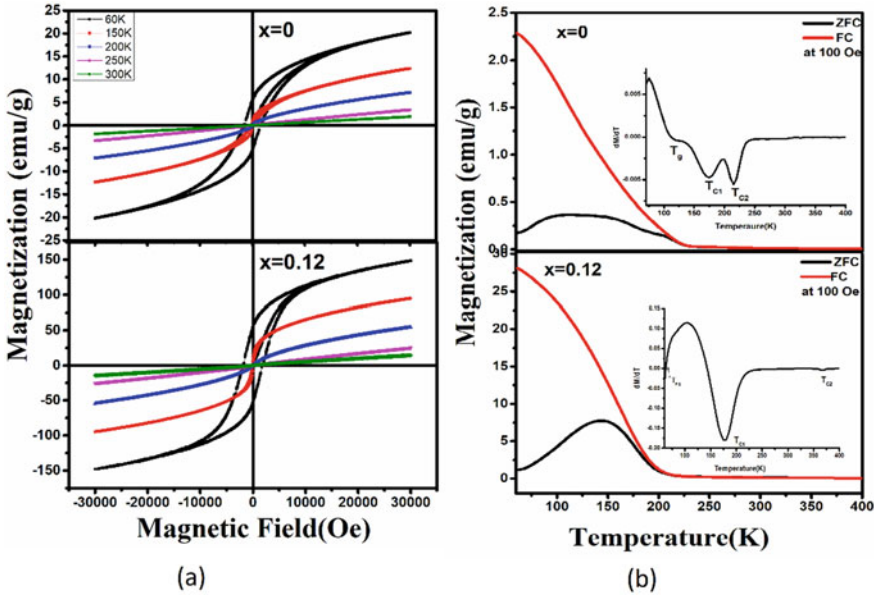


Fig. 8 **a** Magnetization curve of LCMO and LSCMO nanoparticles at 60, 150, 200, 250 and 300 K. **b** ZFC and FC curve at 100 Oe in temperature range 60–400 K. The inset shows the first derivative of ZFC magnetization values plotted as a function of temperature

The anomaly observed at ~ 360 K for Sr doped LCMO could be understood in terms of the effect of hole doping by Sr^{2+} at A site. Due to hole doping at A site, the valence of the B site ions i.e., Co/Mn can be affected [25]. As reported by Lan and coworkers [26] in their theoretical work that holes introduced by Sr doping in LCMO mainly go to oxygen sites and hence Mn^{3+} ions are introduced which disrupts the long-range ordering of Co and Mn [10]. Mn^{3+} ions with valence configuration $3d^4$, due to Jahn Teller effect spontaneously distorts the octahedron as it is energetically favorable, the increment in elastic energy due to distortion of octahedron is balanced by the energy saved due to lowering of e_g orbitals [12]. Mn^{3+} can interact ferromagnetically with the neighboring cation via double exchange mechanism. The transfer of electrons from Mn^{3+} to neighboring ion saves kinetic energy and is allowed only if both are ferromagnetically aligned [12]. Many researchers have reported the existence of ferromagnetic correlations above the Curie temperature for Sr doped manganites [1, 25]. The inverse susceptibility plots and the $d\chi^{-1}/dT$ curves for LSCMO ($x = 0.12$) (inset of Fig. 9) indicate that above the ferromagnetic to paramagnetic transition temperature the behavior is not purely paramagnetic but ferromagnetic correlations exist and we obtain two peaks in $d\chi^{-1}/dT$ versus T graph namely at 368 and 385 K which could be due to varying stoichiometry of oxygen in the compound [26]. The existence of ferromagnetic correlations is evidence of the existence of Griffith like phase [1, 10, 25]

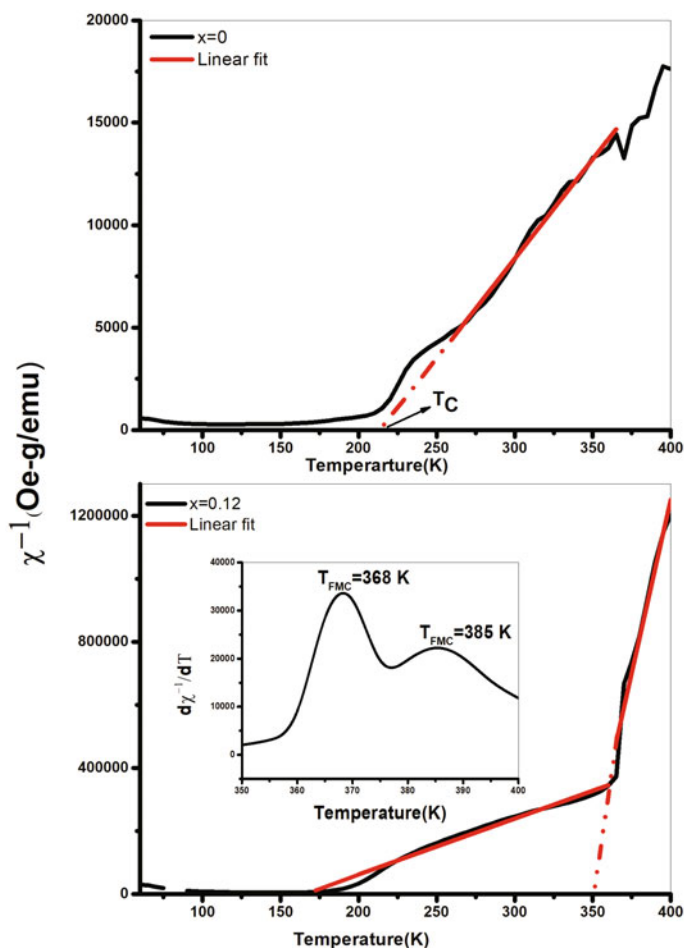


Fig. 9 **a** Inverse susceptibility versus T plot for LCMO nanoparticles, red line indicates linear fit according to Curie Weiss law. **b** Inverse susceptibility versus T plot for LSCMO nanoparticles, red line indicates linear fit according to Curie Weiss law, inset plots derivative of inverse of susceptibility with respect to temperature

4 Conclusion

Double perovskites $\text{La}_2\text{CoMnO}_6$ (LCMO) and $\text{La}_{1.88}\text{Sr}_{0.12}\text{CoMnO}_6$ (LSCMO) have been synthesized successfully using the wet chemical synthesis method of sol-gel. The crystallite size estimated from the peaks of X-ray diffraction pattern using Debye Scherrer formula is around 6–18 nm. Rietveld refinement of X-ray diffraction pattern indicates formation of rhombohedral phase (S.G. No. R3c; 161). The Williamson Hall plots indicate that the strain reduces on doping with Sr in LSCMO nanoparticles. The FTIR and Raman spectra show characteristic bands corresponding to

Co/MnO₆ octahedra further confirming the formation of double perovskite structure. The magnetization study at room temperature shows paramagnetic nature of prepared compounds. From the temperature-dependent magnetization studies, we conclude that multiple interactions between the different oxidation states of B site ions exist. For LSCMO nanoparticles a Griffith like phase above curie temperature exists at 368 K which is useful for spintronics applications.

Acknowledgements The financial support received from the UGC in the form of UGC-BSR research start up grant (F.30-374/2017(BSR)), New Delhi, India is acknowledged. The authors are thankful to the Department of Physics, Banasthali Vidyapeeth and IIT Patna for characterization facilities provided.

References

1. Palakkal JP et al (2015) Observation of high-temperature magnetic transition and existence of ferromagnetic short-range correlations above transition in double perovskite La₂FeMnO₆. RSC advances 5(128):105531–105536
2. Kobayashi K-I et al (1998) Room-temperature magnetoresistance in an oxide material with an ordered double-perovskite structure. Nature 395(6703):677–680
3. Baettig P, Ederer C, Spaldin NA (2005) First principles study of the multiferroics BiFeO₃, Bi₂FeCrO₆, and BiCrO₃: structure, polarization, and magnetic ordering temperature. Phys Rev B 72(21):214105
4. Anderson MT, Greenwood KB, Taylor GA, Poeppelmeier KR (1993) B-cation arrangements in double perovskites. J Solid State Chem 22:197–233
5. Balcells LI, Navarro J, Bibes M, Roig A, Martínez B, Fontcuberta J (2001) Appl Phys Lett 78:781
6. Balcells LI et al (2001) Cationic ordering control of magnetization in Sr₂FeMoO₆ double perovskite. Appl Phys Lett 78(6):781–783
7. Murthy JK et al (2016) Antisite disorder driven spontaneous exchange bias effect in La_{2-x}Sr_xCoMnO₆ (0 ≤ x ≤ 1). J Phys: Condens Matter 28(8):086003
8. Mao Y, Parsons J, McCloy JS (2013) Magnetic properties of double perovskite La₂BMnO₆ (B = Ni or Co) nanoparticles. Nanoscale 5(11):4720–4728
9. Barrozo P, Albino Aguiar J (2013) Ferromagnetism in Mn half-doped LaCrO₃ perovskite. J Appl Phys 113(17):17E309
10. Khan A et al (2018) Effect of Sr-doping on electronic and magnetic properties of La_{2-x}Sr_xCoMnO₆. In: AIP conference proceedings 1942. No. 1. AIP Publishing LLC
11. Mandal PR, Nath TK (2015) Evolution of griffith phase in hole doped double perovskite La_{2-x}Sr_xCoMnO₆ (x = 0.0, 0.5, and 1.0). Mater Res Express 2(6):066101
12. Shahee Aga, et al (2015) Evidence of ferromagnetic short-range correlations in cubic La_{1-x}Sr_xMnO_{3-δ} (x = 0.80, 0.85) above antiferromagnetic ordering. Phys Status Solidi (b) 252(8):1832–1838
13. Blundell S (2003) Magnetism in condensed matter 94–95
14. Patterson AL (1939) The Scherrer formula for X-ray particle size determination. Phys Rev 56(10):978
15. Kumar M, Prajapati B, Singh A (2020) B-site ordering effect on structural and magnetic properties of ‘Y’-modified double perovskite La₂NiMnO₆ nanoparticles. J Mater Sci: Mater Electron 31(10):8099–8105
16. <https://www.taylorfrancis.com/chapters/edit/>, <https://doi.org/10.1201/9781003197492-13/nanoscale-characterization-arvind-kumar-swati-manish-kumar-neelabh-srivastava-anadi-krishna-atul>

17. Sadhu S, Chowdhury PS, Patra A (2008) Synthesis and time- resolved photoluminescence spectroscopy of capped CdS nanocrystals. *J Lumin* 128(7):1235–1240
18. Saberi A et al (2008) Chemical synthesis of nanocrystalline magnesium aluminate spinel via nitrate–citrate combustion route. *J Alloy Compd* 462(1–2):142–146
19. Dass RI, Yan J-Q, Goodenough JB (2003) Oxygen stoichiometry, ferromagnetism, and transport properties of $\text{La}_{2-x}\text{NiMnO}_{6+\delta}$. *Phys Rev B* 68(6):064415
20. Harbi A et al (2021) Tailoring the Griffiths-like cluster formation in the insulator ferromagnet spin-glass $\text{Gd}_2\text{Ni}_x\text{Co}_{1-x}\text{MnO}_6$ double perovskite. *Phys Rev B* 104(5):054404
21. Kumar D, Sathé VG (2015) Raman spectroscopic study of structural transformation in ordered double perovskites $\text{La}_2\text{CoMnO}_6$ bulk and epitaxial film. *Solid State Commun* 224:10–14
22. Magray MA, Ikram M (2019) Dielectric and Raman spectroscopy study of structural phase transformation of Sr-doped $\text{La}_2\text{CoMnO}_6$ double perovskite. *J Mater Sci: Mater Electron* 30(9):8655–8666
23. Truong KD et al (2007) Impact of Co/ Mn cation ordering on phonon anomalies in $\text{La}_2\text{CoMnO}_6$ double perovskites: Raman spectroscopy. *Phys Rev B* 76(13):132413
24. Dass RI, Goodenough JB (2003) Multiple magnetic phases of $\text{La}_2\text{CoMnO}_{6-\delta}$ ($0 < \delta < 0.05$). *Phys Rev B* 67(1):014401
25. Eglitis RI (2014) Ab initio calculations of SrTiO_3 , BaTiO_3 , PbTiO_3 , CaTiO_3 , SrZrO_3 , PbZrO_3 and BaZrO_3 (001), (011) and (111) surfaces as well as F centers, polarons, KTN solid solutions and Nb impurities therein. *Int J Mod Phys B* 28(17):1430009
26. Lan X, Kong S, Zhang WY (2011) Theoretical study on the electronic and magnetic properties of double perovskite $\text{La}_{2-x}\text{Sr}_x\text{MnCoO}_6$ ($x = 0, 1, 2$). *Eur Phys J B* 84:357–364